Journal of Computational Physics 229 (2010) 2093–2108

Contents lists available at ScienceDirect

Journal of Computational Physics

journal homepage: www.elsevier.com/locate/jcp

Wavelet frame based scene reconstruction from range data

Hui Ji [a,*], Zuowei Shen [a], Yuhong Xu [b]

[a] Department of Mathematics, National University of Singapore, Singapore 117542, Singapore
[b] Center for Wavelets, Approx. and Info. Proc., National University of Singapore, Singapore 117542, Singapore

ARTICLE INFO

Article history:
Received 28 August 2009
Received in revised form 11 November 2009
Accepted 12 November 2009
Available online 27 November 2009

Keywords:
Scene reconstruction
Piecewise smooth function
Tight frame
Sparse representation
Split Bregman method

ABSTRACT

How to reconstruct the scene (a visible surface) from a set of scattered, noisy and possibly sparse range data is a challenging problem in robotic navigation and computer graphics. As most real scenes can be modeled by piecewise smooth surfaces, traditional surface fitting techniques (*e.g.* smoothing spline) generally can not preserve sharp discontinuities of surfaces. Based on sparse approximation of piecewise smooth functions in frame domain, we propose a new tight frame based formulation for reconstructing a piecewise smooth surface from a sparse range data set, which is robust to both additive noise and outliers. Furthermore, the resulting minimization problem from our formulation can be efficiently solved by the split Bregman method [1,2]. The numerical experiments show that the proposed approach is capable of reconstructing a piecewise smooth surface with sharp edges from sparse range data corrupted with noise and outliers.

1. Introduction

High-quality 3D scene modeling has long been an important research topic in computer vision, robotic navigation, computer graphics and animation. The 3D geometrical model of a scene is usually reconstructed from pre-acquired range data sets of the scene. There are two types of 3D range data acquisition technologies. One is active scanning technology that directly captures 3D range data sets using laser or medical scanners; the other is passive scanning technology that derives 3D range information from photometric images of the scene using computer vision based methods, *e.g.* shape from shading, structure from motion and stereo imaging. There are significant differences in terms of quality and accuracy among range data sets acquired from different acquisition technologies. Digital entertainment industry and computer graphics researchers have been using advanced 3D laser scanners to acquire complete and dense 3D range data sets of scenes. However, those instruments are very costly and bulky which make them unsuitable for many mobile applications such as mobile robot navigation. In contrast, those compact and affordable laser rangefinders can only produce low-resolution range images which are error-prone in practice. Computer vision based approaches also provide an affordable solution to acquire 3D range data by using photometric images captured by optical cameras. However, 3D points produced by computer vision techniques are usually very noisy, with a lot of outliers and sparsely distributed in the 3D space with large gaps.

In the past, there have been extensive researches on reconstructing objects or scenes using range data from a single view or from multiple views. Interested readers are referred to a recent survey [3, Chapter 4] for more details. In this paper, we focus on how to reconstruct the scene model using 3D range data of a single view. Because the range data from a single view can only provide 3D information for visible surfaces of the scene, a piecewise smooth explicit surface model is usually adequate to describe visible surfaces of a scene in most scenarios. It is noted that the discontinuities of the reconstructed piecewise smooth surface provide very important information for many applications (*e.g.* robotics), as the discontinuities of the

* Corresponding author. Tel.: +65 65168845; fax: +65 67795452.
E-mail addresses: matjh@nus.edu.sg (H. Ji), matzuows@nus.edu.sg (Z. Shen), tslxyh@nus.edu.sg (Y. Xu).

0021-9991/$ - see front matter © 2009 Elsevier Inc. All rights reserved.
doi:10.1016/j.jcp.2009.11.024

surface either represent the boundaries of objects in the scene or denote the sharp geometrical shape changes of individual objects. Thus, a desired reconstruction algorithm should preserve surface discontinuities well without over-smoothing these regions as most traditional surface fitting methods tend to do. Moreover, we concentrate on those 3D range data sets which are either obtained from low-cost time-of-flight laser rangefinders or estimated from photometric data using computer vision techniques. As these data sets are very noisy, corrupted with a lot of outliers, sparsely sampled with large gaps, this paper aims at developing an efficient piecewise smooth surface reconstruction algorithm from a sparse range data set, which is robust to all the noises and preserves surface discontinuities well.

Reconstructing a piecewise smooth surface using range data can be formulated as a functional reconstruction problem. Assume that we are given a set of scattered data sites:

$$\Xi = \{x_1, x_2, \ldots, x_n\} \subset \mathbb{R}^2$$

and associated function values

$$f|_\Xi = \{f_1, f_2, \ldots, f_n\},$$

where f_i is the function value of an unknown data function $f(x)$ at x_i and possibly contains noise, i.e.

$$f_i = f(x_i) + \epsilon_i.$$

Our goal is then to reconstruct the data function f under the assumption that f is a piecewise smooth function. It is emphasized that the discontinuities of f need to be well preserved in the reconstruction, because they encode important information about boundaries of objects on which many high-level tasks depend, Also, the input data sites Ξ can be scattered such that they are non-uniformly sampled, with large gaps and even sparse (few samples available). And the obtained function values $f|_\Xi$ could be very noisy. All these challenges make the reconstruction a difficult problem.

Among all available functional reconstruction methods, smoothing spline is one of the most widely used methods. The smoothing spline of order m in $\mathbb{R}^d$ is posed as the solution of the following regularized least squares problem:

$$\min_g \quad \sum_{i=1}^{n} (g(x_i) - f_i)^2 + \lambda |g|^2_{H^m}, \quad g \in H^m, \tag{1}$$

where the first least squares term measures the fitting error, and the second regularization term measures the roughness of g by using the semi-norm associated with the Beppo-Levi space H^m in $\mathbb{R}^d$, i.e. $|g|_{H^m}$ (see *e.g.* [4]). The parameter $\lambda > 0$, the regularization (or smoothing) parameter, adjusts the balance between data fidelity and regularization. Smoothing spline method has been successfully applied on solving scattered data approximation problems in a wide range of applications (*e.g.* [5,6]).

In this paper, we are interested in surface reconstruction, i.e. the case $d = 2$. The performance of smoothing spline is good when the underlying surface is smooth. However, the corresponding computation becomes very expensive when the number of data sites n grows large, because of the global support of basis functions and the ill-conditionedness of the resulting linear system. Motivated by the works in [7–9] which use a simple principal shift invariant space and its associated wavelet transform to fit scattered data, [4] proposed an efficient algorithm to approximate the solution of smoothing spline in a principal shift invariant space.

Let $\Omega \subset \mathbb{R}^2$ be a bounded domain of interest where all data sites lie in, and let ϕ be a carefully chosen, compactly supported continuous function (*e.g.* uniform B-splines, box splines, nodal basis functions), we look for fitting functions in the space spanned by those h-dilates and h-shifts of ϕ whose support intersects Ω, i.e.

$$S^h(\phi, \Omega) = \left\{ \sum_{k \in \mathbb{Z}^2} c(k)\phi(\cdot/h - k) : c(k) = 0 \text{ whenever } \operatorname{supp}\phi(\cdot/h - k) \cap \Omega = \emptyset \right\},$$

where $h > 0$ is a scaling parameter that controls the refinement of the space. Then any fitting function $s(x) \in S^h(\phi, \Omega)$ can be written as a finite expansion:

$$s(x) = \sum_{k \in \mathcal{I}} u_k \phi(x/h - k), \tag{2}$$

where $\mathcal{I} := \{k \in \mathbb{Z}^2 : \operatorname{supp}\phi(\cdot/h - k) \cap \Omega = \emptyset\}$. Let $\boldsymbol{u}$ and $\boldsymbol{f}$ denote the column vector $[u_k]_{k \in \mathcal{I}}$ and $[f_i]_{1 \leqslant i \leqslant n}$, respectively. In this finite dimensional space $S^h(\phi, \Omega)$, the smoothing spline formulation (1) can be approximated by the following minimization

$$\min_{\boldsymbol{u}} \quad \frac{1}{2}\|A\boldsymbol{u} - \boldsymbol{f}\|_2^2 + \lambda \boldsymbol{u}^T G \boldsymbol{u}, \tag{3}$$

where A is the observation matrix defined by

$$A(i,k) = \phi(x_i/h - k), \quad i = 1, 2, \ldots, n, \ k \in \mathcal{I}, \tag{4}$$

G is a nonnegative definite matrix such that $|s|^2_{H^m(\Omega)} = \boldsymbol{u}^T G \boldsymbol{u}$ (see [4]). Several desirable properties that the space $S^h(\phi, \Omega)$ enjoys motivated us to choose it as an approximation space for fitting a smooth curve or surface to scattered data points. First, it has a simple structure and provides good approximation to smooth functions as proved in [4], which naturally leads to

simple and accurate algorithms. The quality of the obtained fitting function is very much equivalent to that of smoothing spline, but it is done in a much more efficient way by using simpler basis functions. Furthermore, it can be associated to a wavelet or frame system and hence one can solve the data fitting problem by making use of the advantages that a wavelet (frame) system can offer. These advantages include sparse approximation of functions in the wavelet (frame) domain, multilevel structure of basis functions, adaptivity to the data, norm equivalence, etc. In [4], the Sobolev norm equivalence plays an important role in the design of the efficient algorithm for smooth function reconstruction.

It has been observed in many literatures (*e.g.* [10,11]) that when ℓ_2-norm regularization term is applied to the data set whose underlying function or surface is piecewise smooth, the resulting solution tends to be smooth without sharp discontinuities, as well as undesirable oscillations around the discontinuities. Hence, the smoothing spline method or the method given in [4] is not suitable for our purpose here because what we are seeking for is a piecewise smooth solution which preserves sharp discontinuities. Recently, several surface reconstruction approaches have been proposed to preserve surface discontinuity by replacing ℓ_2 regularization using more sophisticated regularization, *e.g.* the Huber approximation of ℓ_1-norm of function derivatives in [11], the local kernel regularization in [12] and the non-local means regularization in [13].

In the approach taken here, we continue employing the shift invariant space $S^h(\phi, \Omega)$ and its associated wavelet frame system. It is the same spirit of using an approximation space with simple structure to reconstruct the underlying function or surface from the given data set. However, we will seek a sparse solution of the problem in the wavelet frame domain by using the fact that piecewise smooth functions can be approximated sparsely by wavelet frames. Let ϕ be a refinable function from which a wavelet tight frame system can be constructed, *e.g.* 2D tensor product of a uniform B-spline as used in [4]; see Section 2 for a short introduction of wavelet tight frame systems. With this choice of ϕ, we can represent the fitting function $s(x)$ in (2) in an associated wavelet tight frame system when $h = 1/2^J$ for some positive integer J. Let W be a wavelet frame transform which transforms the coefficient vector $\boldsymbol{u}$ to the tight frame coefficient vector $W\boldsymbol{u}$ (this W is also called an analysis operator in the frame theory). To find a solution in $S^h(\phi, \Omega)$ which is sparse in terms of its tight frame coefficients, we take the following so-called analysis based approach in imaging science (*e.g.* [1,14–16]), i.e. to find a vector $\boldsymbol{u}$ satisfying

$$\min_{\boldsymbol{u}} \quad \frac{1}{2}\|A\boldsymbol{u} - \boldsymbol{f}\|_2^2 + \|\mathrm{diag}(\boldsymbol{\lambda})W\boldsymbol{u}\|_1, \tag{5}$$

where A is the observation matrix defined in (4), $\mathrm{diag}(\boldsymbol{\lambda})$ is a diagonal matrix with the diagonal being the vector $\boldsymbol{\lambda}$, and $\|\cdot\|_1$ denotes the ℓ_1-norm. The first term in this minimization, as usual, characterizes the fitting error. The second regularization term $\|\mathrm{diag}(\boldsymbol{\lambda})W\boldsymbol{u}\|_1$ penalizes the roughness of the solution on one hand, and preserves discontinuities on the other hand. We will give a more detailed discussion on this in the next section.

The type of the minimization problem (5) (with general A and W) encompasses many important formulations in imaging science and other computational areas, see *e.g.* [1,2]. The split Bregman method proposed in [2] has been proved to be very efficient in solving (5) with various successful applications in imaging sciences, see *e.g.* [1,2,17]. All these observations motivate us to adopt the wavelet frame based method (5) to solve the surface reconstruction problem and use the split Bregman method as a numerical solver of (5).

The remainder of this paper is organized as follows. Section 2 is devoted to the formulation of wavelet frame based method and the corresponding algorithm for function or surface reconstruction. Numerical simulations and experiments are given in Section 3.

2. Surface reconstruction by wavelet tight frame

This section is devoted to the formulation and the algorithm of our wavelet frame based method for functional surface reconstructions. we start with a brief introduction of wavelet tight frame.

2.1. Wavelet tight frames

We present here some basics of wavelet tight frames. Interested readers should consult [18–21] and the references therein to get a complete picture of it. The wavelet tight frames used here are mainly in two variable setting, however, for simplicity, we only present wavelet tight frames in the univariate setting, since we use tensor product wavelet frames in the implementation.

A countable subset of $X \subset L_2(\mathbb{R})$ is called a *tight frame* of $L_2(\mathbb{R})$ if

$$f = \sum_{g\in X}\langle f, g\rangle g, \quad \forall\, f \in L_2(\mathbb{R}). \tag{6}$$

This is equivalent to

$$\|f\|^2 = \sum_{g\in X}|\langle f, g\rangle|^2, \quad \forall\, f \in L_2(\mathbb{R}),$$

where $\langle\cdot,\cdot\rangle$ and $\|\cdot\|$ denote the inner product and the norm of $L_2(\mathbb{R})$. Tight frame, as a generalization to orthonormal basis, relaxes the requirement of X being a basis of $L_2(\mathbb{R})$ and brings in redundancy that has been proved useful in many applications in signal and image processing (see *e.g.* [22,23]). Since tight frame is redundant, there are an infinite number of possible

expansions of f in the system X. The particular expansion given in (6) is called the canonical expansion, and $\{\langle f, g\rangle\}$ is the canonical frame coefficient sequence.

A wavelet system $X(\Psi)$ is defined to be a collection of dilations and shifts of a finite set $\Psi = \{\psi^1, \ldots, \psi^r\} \subset L_2(\mathbb{R})$,

$$X(\Psi) := \{\psi_{j,k} := 2^{j/2}\psi(2^j \cdot -k), \quad j \in \mathbb{Z},\ k \in \mathbb{Z}, \psi \in \Psi\}.$$

When $X(\Psi)$ forms a tight frame, it is called a *wavelet tight frame* and each $\psi \in \Psi$ is called a *framelet*. To construct compactly supported wavelet tight frames, one usually starts with a compactly supported refinable function ϕ (called a scaling function) with a refinement mask τ_0 satisfying

$$\hat{\phi}(2\cdot) = \tau_0\hat{\phi},$$

where $\hat{\phi}$ is the Fourier transform of ϕ, and τ_0 is a 2π-periodic trigonometric polynomial with $\tau_0(0) = 1$. For a given compactly supported refinable function ϕ, the construction of a wavelet tight frame is to find an appropriate set of framelets $\Psi = \{\psi^1, \ldots, \psi^r\}$ defined in the Fourier domain by

$$\hat{\psi}^i(2\cdot) = \tau_i\hat{\phi}, \quad i = 1, 2, \ldots, r,$$

where the framelet masks τ_i's are 2π-periodic trigonometric polynomials. The Unitary Extension Principle (UEP) of [21] says that $X(\Psi)$ forms a tight frame provided that

$$\tau_0(\omega)\overline{\tau_0(\omega+\gamma\pi)} + \sum_{i=1}^{r}\tau_i(\omega)\overline{\tau_i(\omega+\gamma\pi)} = \delta_{\gamma,0}, \quad \gamma = 0, 1.$$

As an application of UEP, a family of wavelet tight frame systems is derived in [21] by using uniform B-splines as the refinable function ϕ. The simplest system in this family is piecewise linear B-spline tight frame which uses piecewise linear B-spline function as ϕ. This ϕ has the refinement mask $\tau_0 = \cos^2\left(\frac{\omega}{2}\right)$, and the corresponding low-pass filter is

$$\boldsymbol{h}_0 = \frac{1}{4}[1, 2, 1].$$

Two framelets ψ_1, ψ_2 are defined by the framelet masks $\tau_1 = -\frac{\sqrt{2}i}{2}\sin(\omega)$ and $\tau_2 = \sin^2\left(\frac{\omega}{2}\right)$, whose corresponding high-pass filters are

$$\boldsymbol{h}_1 = \frac{\sqrt{2}}{4}[-1, 0, 1], \quad \boldsymbol{h}_2 = \frac{1}{4}[-1, 2, -1]. \tag{7}$$

The plot of $\phi,\ \psi_1,\ \psi_2$ is given in Fig. 1. Other constructions of wavelet tight frames from higher-order uniform B-splines can be found in [21]. For the numerical implementation in this paper, we will only use the piecewise linear B-spline tight frame. The effectiveness of this simple piecewise linear B-spline tight frame has been demonstrated in image restoration [1,24–27]. We will show in this paper that such a simple system can also be used to effectively reconstruct piecewise smooth surface from a scattered data set.

It is known that the weighted norm of the canonical frame coefficient sequence of a function is equivalent to its function norm in some spaces, *e.g.* Sobolev or Besov spaces (see [18,20] for more details). In particular, it is shown in [18] that the ℓ_1-norm of the canonical frame coefficient sequence of a function, used as a regularization in (5), is equivalent to its Besov norm under some mild conditions on framelets. Therefore, the regularization term $\|\mathrm{diag}(\boldsymbol{\lambda})W\boldsymbol{u}\|_1$ in (5) penalizes the roughness of the solution. It also preserves sharp discontinuities, since the ℓ_1-norm minimization annihilates small coefficients in the wavelet frame domain, which is well-known to be able to keep sharp edges. Furthermore, since the canonical expansion (6) of a tight wavelet system can be sparse (i.e. large number of canonical coefficients are equal or close to zero and negligible, see [18,20]) for a large class of functions, such as piecewise smooth functions, we still get a good approximation by neglecting small coefficients.

Numerical computation of the wavelet frame transform is done by using the wavelet frame decomposition algorithm given in [19]. In fact, we use the decomposition algorithm without down-sampling. This can be easily implemented by using the refinement and framelet masks. The transform can be represented by a matrix W whose construction depends on the boundary conditions. In this paper, we use the Neumann (symmetric) boundary condition. Since [25,28] have given details

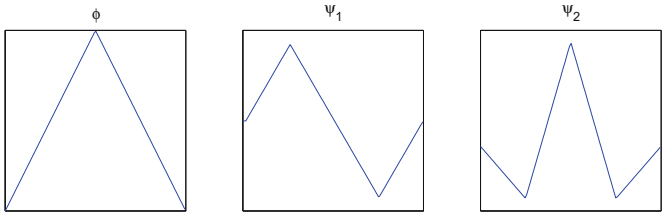

Fig. 1. The piecewise linear B-spline tight frame system.

of how to generate such matrix, we omit the detailed discussions here and the interested reader should consult [25,28] for details.

With the matrix W, it is easy to describe the transformation process. Let $\boldsymbol{u}$ be a vector of scaling coefficients as a given set of sample data, the frame coefficient vector $\boldsymbol{v}$ can be computed via

$$\boldsymbol{v} = W\boldsymbol{u}.$$

Once we have W, the inverse transform, i.e. the reconstruction algorithm, is W^T, i.e.

$$\boldsymbol{u} = W^T\boldsymbol{v}.$$

It is very important to note that W can be constructed from the refinement and framelet masks such that $W^TW = I$. The rows of the matrix W form a tight frame in a finite dimension space which connects well to the wavelet frame system in function spaces (see *e.g.* [19] for details). In general, since there are more rows than columns in W, $WW^T \neq I$. When $WW^T = I$, then the rows of W form an orthonormal basis. Finally we remark that in practical computation, we are working in the bivariate setting. We employ the tensor product of 1D wavelet tight frame, and the corresponding matrix W can be constructed easily via the Kronecker product of the matrix constructed by univariate wavelet frame transform (see [28] for details). In the rest of this paper, we still use W to denote the discrete transform generated by bivariate wavelet tight frame. We further note that the W is basically used for notational convenience, in the computation, we do not use matrix multiplication. Instead, we use a wavelet decomposition and reconstruction algorithm directly modified from [19].

2.2. Formulation

For a given set of scattered sites $\{x_i\}_{i=1}^n \subset \Omega \subset \mathbb{R}^2$ and the corresponding data $\{f_i\}_{i=1}^n$, our task is to reconstruct a fitting surface. We assume that Ω is a rectangle, as the interested domain Ω is often rectangular in scene reconstruction, Let ϕ be the 2D tensor product of a uniform B-spline function, and let $h = 1/2^J$ be the scaling parameter for some positive integer J, determined by the density of scattered sites. For example, in our implementation, J is set to 7 when the scattered data is defined on a 128×128 grid.

We then look for a function in $S^h(\phi, \Omega)$ which fits closely to the given data and at the same time preserves sharp discontinuities. Since any function $s(x) \in S^h(\phi, \Omega)$ can be written as

$$s(x) = \sum_{k\in\mathcal{I}} u_k\phi(2^Jx - k), \quad \text{where } \mathcal{I} := \{k \in \mathbb{Z}^2 : \operatorname{supp}\phi(2^J\cdot - k) \cap \Omega = \emptyset\}.$$

$s(x)$ is completely determined by the coefficient vector $\boldsymbol{u} = [u_k]_{k\in\mathcal{I}}$. Let $\boldsymbol{f} = [f_i]_{1\leqslant i\leqslant n}$ and A be the observation matrix defined by

$$A(i,k) = \phi(2^Jx_i - k), \quad i = 1,2,\ldots,n,\ k \in \mathcal{I}.$$

To seek for the fitting function $s(x)$, we propose the following minimization problem:

$$\min_{\boldsymbol{u}} \quad H(\boldsymbol{u}) + \|\operatorname{diag}(\boldsymbol{\lambda})W\boldsymbol{u}\|_1. \tag{8}$$

Here the matrix W is a discrete wavelet frame transform associated with the bivariate B-spline tight frame. Note that $W\boldsymbol{u}$ is the canonical frame coefficient sequence of $s(x)$, hence the regularization term $\|\operatorname{diag}(\boldsymbol{\lambda})W\boldsymbol{u}\|_1$ penalizes the roughness of the fitting function $s(x)$, and it also encourages to preserve sharp edges as it is biased to sparse solution of $s(x)$. We note that the matrix W is constructed via the Neumann boundary condition, which implies that the symmetric boundary condition is used to extend $\boldsymbol{u}$ across the boundaries of Ω. The mos popular choice for the data fidelity term $H(\boldsymbol{u})$ is the ℓ_2-norm of fitting error:

$$H(\boldsymbol{u}) = \frac{1}{2}\|A\boldsymbol{u} - \boldsymbol{f}\|_2^2. \tag{9}$$

From a statistical point of view, the ℓ_2 fitting term is suitable to data corrupted with Gaussian noise. However, there are usually a lot of outliers in the data for the scene reconstruction (see *e.g.* [29]) and it is known that the ℓ_2 norm is sensitive to outliers. In such a case, we use the ℓ_1 data fidelity term:

$$H(\boldsymbol{u}) = \|A\boldsymbol{u} - \boldsymbol{f}\|_1.$$

The implications of the ℓ_1 data fidelity term have been studied in many research papers (*e.g.* [30,31]). In particular, [31] justified the use of ℓ_1 data fitting term for processing data corrupted with outliers in both theoretical analysis and numerical experiments. Roughly speaking, due to its quadratic growth rate, the ℓ_2-norm fitting does not encourage large deviations from the given data points and naturally leads to a close fit to the outliers; in contrast, because of its comparatively lower growth rate, the ℓ_1-norm fitting promotes sparsity and allows large deviations, thus the bias effect of outliers is effectively alleviated. In our numerical implementation, we approximate the non-differentiable ℓ_1 fitting term by its smoothed version

$$H(\boldsymbol{u}) = \sum_{i=1}^{n}\sqrt{(A\boldsymbol{u} - \boldsymbol{f})_i^2 + \alpha}, \tag{10}$$

where α is a small positive number.

2.3. Algorithm

In this section, we use the split Bregman algorithm to solve the resulting minimization problem from our surface fitting formulation. Essentially, we need to find a solution $\boldsymbol{u}$ that satisfies

$$\min_{\boldsymbol{u}} \quad E(\boldsymbol{u}) = H(\boldsymbol{u}) + \|D\boldsymbol{u}\|_1, \tag{11}$$

where $D = \mathrm{diag}(\lambda)W$ and

$$H(\boldsymbol{u}) = \frac{1}{2}\|A\boldsymbol{u} - \boldsymbol{f}\|_2^2, \quad \text{or} \quad \sum_{i=1}^{n}\sqrt{(A\boldsymbol{u} - \boldsymbol{f})_i^2 + \alpha}.$$

If general H and D are considered, this type of the minimization problems (11) encompasses many important formulations in imaging science and other computational areas, see *e.g.* [1,2]. Numerical solution to such minimization problems was previously known to be very computationally challenging. However, the *split Bregman iteration* developed in [2] has been shown to be a very efficient tool for solving (11). The Bregman iteration was first introduced to image processing community in [32] where it was applied to the ROF denoising model. It was then applied to a variety of signal and image processing problems such as basis pursuit [33] and frame based image restoration [34]. The split Bregman iteration extends utility of the Bregman iteration for a more general class of ℓ_1 minimization problems. Its basic idea is to convert the unconstrained minimization problem (11) into a constrained one by introducing an auxiliary variable $\boldsymbol{d} = D\boldsymbol{u}$ and then invoke the Bregman iteration to solve the constrained minimization problem. This algorithm connects to some existing algorithms in optimization, as pointed out by [35,36]. In fact, the split Bregman algorithm is equivalent to the alternating direction method of multipliers [37,38] and the Douglas–Rachford splitting algorithm for the dual problem, see *e.g.* [39–41]. The split Bregman algorithm has several attractive features for our application. It converges fast, uses a small memory footprint and is easy to code, as illustrated in the numerical simulations of [1,2]. The algorithm adapted to our minimization problem (11) is given as follows.

Let $\boldsymbol{u}^0 = 0,\ \boldsymbol{d}^0 = \boldsymbol{b}^0 = 0$, be the initial seeds, the split Bregman algorithm for (11) is given as follows:

$$\begin{cases} \boldsymbol{u}^{k+1} = \arg\min_{\boldsymbol{u}} H(\boldsymbol{u}) + \frac{\mu}{2}\|D\boldsymbol{u} - \boldsymbol{d}^k + \boldsymbol{b}^k\|_2^2, \\ \boldsymbol{d}^{k+1} = T_{1/\mu}(D\boldsymbol{u}^{k+1} + \boldsymbol{b}^k), \\ \boldsymbol{b}^{k+1} = \boldsymbol{b}^k + (D\boldsymbol{u}^{k+1} - \boldsymbol{d}^{k+1}), \end{cases} \tag{12}$$

where $\mu > 0$ is a parameter of the algorithm, T_θ is the soft-thresholding operator defined by

$$T_\theta : \boldsymbol{x} = [x_1, x_2, \ldots, x_M] \ \rightarrow\ T_\theta(\boldsymbol{x}) = [t_\theta(x_1), t_\theta(x_2), \ldots, t_\theta(x_M)],$$

where

$$t_\theta(\xi) = \mathrm{sgn}(\xi)\max\{0, |\xi| - \theta\}.$$

The stopping criteria for the split Bregman iteration (12) is posed as $\|\boldsymbol{d}^k - D\boldsymbol{u}^k\| \leqslant \epsilon$ with ϵ being a given tolerance. Since the first term H in (11) has two different choices, correspondingly, the first step of each iteration in (12) is either

$$(A^TA + \mu D^TD)\boldsymbol{u} = A^T\boldsymbol{f} + \mu D^T(\boldsymbol{d}^k - \boldsymbol{b}^k) \tag{13}$$

or

$$\min_{\boldsymbol{u}} \quad \sum_{i=1}^{n}\sqrt{(A\boldsymbol{u} - \boldsymbol{f})_i^2 + \alpha} + \frac{\mu}{2}\left\|D\boldsymbol{u} - \boldsymbol{d}^k + \boldsymbol{b}^k\right\|_2^2. \tag{14}$$

The linear system in (13) is positive definite and therefore it can be solved by the conjugate gradient method. For the minimization in (14), since its objective functional is differentiable, it can be solved by the standard gradient descent method. One aspect of split Bregman iteration that contributes to its efficiency is that it is unnecessary to solve the first subproblem, i.e. (13) or (14) here, to the full convergence. Instead, only a small number of inner iterations are adequate at each split Bregman iteration. For more discussions on efficiency of split Bregman iteration, please refer to [1,2,35]. We remark that although we use a smoothed version of the ℓ_1 data fidelity term in the above robust algorithm, the split Bregman iteration actually can also be used to minimize an energy functional with both ℓ_1 data fidelity term and ℓ_1 regularization term, such as L1-TV norm minimization. The interested reader are referred to [35] for more details.

The following theorem, which follows from [1, Theorem 3.2], says that iteration (12) is the right one to use.

Theorem 1. *Iteration (12) satisfies the following property:*

$$\lim_{k\to\infty} H(\boldsymbol{u}^k) + \|D\boldsymbol{u}^k\|_1 = H(\boldsymbol{u}^*) + \|D\boldsymbol{u}^*\|_1, \tag{15}$$

where $\boldsymbol{u}^*$ is a minimizer of (11), whenever $\lambda > 0$. Furthermore, assume that (11) has a unique minimizer, then iteration (12) converges, i.e.

$$\lim_{k\to\infty} \|\boldsymbol{u}^k - \boldsymbol{u}^*\|_2 = 0. \tag{16}$$

Proof. To apply [1, Theorem 3.2], we need to prove that there exists a minimizer satisfying (11). The existence of such a minimizer follows immediately from the definition of the cost functional. □

Note that the uniqueness of the solution cannot be guaranteed in general. Indeed, the matrix A is not, in general, invertible, since the number of basis functions is normally chosen to be larger than the number of points in order to get a good approximation. Nevertheless, (15) shows that the iteration leads a solution whose cost functional value is close to the minimal value.

3. Numerical experiments

The main purpose of this section is to evaluate the performance of our proposed tight frame based method (8) on reconstructing a piecewise smooth surface from sparse range data. Our experimental results are compared against that from three previously developed methods. Numerical experiments are conducted on both synthetic data sets and real data sets. Also, We evaluate the performance of using the ℓ_2 fitting term and using the ℓ_1 fitting term in (8) in the presence of outliers. In the following section, we give a brief description on three methods chosen for comparison.

3.1. Other methods for comparison

Through the experiments, three representative existing surface fitting methods are chosen to be compared against our proposed method. The first method for comparison is the smoothing spline method. Instead of using traditional smoothing spline approach, we use the one proposed in [4] that is to find a solution in a shift invariant space satisfying (3). It is shown in [4] that this approach reconstructs fitting surfaces which are very similar to that from traditional smoothing spline approaches.

The second method for comparison is total variation (TV) based method. Let Ω be partitioned into an $M \times L$ rectangular mesh. We define a set of nodal basis functions on the mesh: each node (m, l) is associated with a nodal basis function, denoted by $\varphi_{m,l}$, which is a linear function with value 1 at that node and 0 at all other nodes, and the corresponding nodal variable is $\boldsymbol{u}_{m,l}$, $1 \leqslant m \leqslant M$ and $1 \leqslant l \leqslant L$. Here $\boldsymbol{u}$ is denoted by bold face to emphasize that it can be viewed as a matrix, and with a slight abuse of notation, $\boldsymbol{u}$ also denotes the vector (with k as the index) formed by concatenating the columns of the matrix. Similar to the case of the frame based reconstruction, the observation matrix A can be formed by evaluating the nodal basis functions at the given scattered sites, i.e.

$$A(i,k) = [\varphi_{m,l}(x_i)], \quad i = 1, 2, \ldots, n, \ k = (m-1)L + l.$$

Let $\nabla \boldsymbol{u} = (\nabla_x \boldsymbol{u}, \nabla_y \boldsymbol{u})$ be the discrete gradient operator defined by

$$(\nabla \boldsymbol{u})_{m,l} = \left((\nabla \boldsymbol{u})^x_{m,l}, (\nabla \boldsymbol{u})^y_{m,l}\right)$$

with

$$(\nabla \boldsymbol{u})^x_{m,l} = \begin{cases} \boldsymbol{u}_{m+1,l} - \boldsymbol{u}_{m,l} & \text{if } m < M \\ 0 & \text{if } m = M, \end{cases} \quad (\nabla \boldsymbol{u})^y_{m,l} = \begin{cases} \boldsymbol{u}_{m,l+1} - \boldsymbol{u}_{m,l} & \text{if } l < L \\ 0 & \text{if } l = L. \end{cases} \tag{17}$$

The discrete isotropic total variation of $\boldsymbol{u}$ can be defined by

$$\mathrm{TV}(\boldsymbol{u}) = \sum_{m=1}^{M} \sum_{l=1}^{L} \left|(\nabla \boldsymbol{u})_{m,l}\right|,$$

where $|y| := \sqrt{y_1^2 + y_2^2}$, $\forall y = (y_1, y_2) \in \mathbb{R}^2$. Then we get the following regularized TV formulation:

$$\min_{\boldsymbol{u}} \quad \frac{1}{2}\|A\boldsymbol{u} - \boldsymbol{f}\|_2^2 + \lambda \mathrm{TV}(\boldsymbol{u}). \tag{18}$$

This formulation is very similar to the ROF denoising model [16], except that the identity matrix in ROF is replaced by the observation matrix A, due to the non-uniformity of data sites. TV regularization is known to be able to preserve edges in the reconstructed function and has been widely used in many imaging restoration models, see *e.g.* [42]. However, it tends to produce undesirable "staircases" artifacts, which appear more pronounced if the reconstructed function is visualized in terms of a surface rather than an image. The solution to (18) still can be efficiently computed by using split Bregman iteration. Here we do not intend to get into details, instead we refer to [2] for a similar numerical algorithm for the ROF denoising model.

The last piecewise smooth surface fitting method for comparison [11] is closely related to the above TV-based formulation. The method seeks the solution of the following regularized formulation:

$$\min_{\boldsymbol{u}} \quad \frac{1}{2}\|A\boldsymbol{u}-\boldsymbol{f}\|_2^2+\lambda\sum_{i=1}^{r}\sum_{m=1}^{M}\sum_{l=1}^{L}U\Big((\mathcal{D}_i\boldsymbol{u})_{m,l}\Big), \tag{19}$$

where $\mathcal{D}_1,\ldots,\mathcal{D}_r$ is a sequence of difference operators acting on $\boldsymbol{u}$, and U is the Huber function with a positive parameter β:

$$U(\xi)=\begin{cases}\xi^2 & \text{if } |\xi|\leqslant\beta\\ \beta^2+2\beta|\xi-\beta| & \text{if } |\xi|>\beta,\end{cases} \tag{20}$$

which serves as a smooth approximation to the absolute value function, so the regularization in (19) is an approximation of the ℓ_1-norm of derivatives of the underlying function. Our implementation only concerns with the first order difference operator [$\mathcal{D}_1$, $\mathcal{D}_2$ are defined by (17)], and we choose small β such that the regularization term is a good approximation of anisotropic TV-norm. This method is denoted as the Huber-TV method in the following discussion. Its solution can be computed using standard optimization schemes, *e.g.* the gradient descent method, because the objective functional is differentiable. However, it is noted that the convergence rate could be rather slow.

3.2. Synthetic 3D surface example

The first experiment is conducted on a synthetic 3D surface example with analytic expression, a "wedding cake" shape composed of three parallel planes as illustrated in Fig. 2(a). The similar example is also used in [11]. The range data set used in the experiment is synthesized as follows: a set of 1000 points on the 3D shape are randomly sampled and then corrupted by Gaussian noise $N(0,\sigma^2)$ with $\sigma=0.01$. Fig. 2(b) shows a vanilla version of the reconstructed surface from this synthesized data set using nearest neighbor interpolation to illustrate how the noisy samples of the underlying surface look like. Then, the reconstruction results from our proposed algorithm with ℓ_2 norm fitting term and from three other methods are shown in Fig. 2(c)–(f). The regularization parameters used in each method are shown in the corresponding figure, which are chosen by trial-and-error. h is set to 1/128 in this experiment. For the regularization factor diag(λ) in our wavelet frame based method, we set those parameters corresponding to scaling coefficients to a very small number and all the others to a constant λ.

It is not surprising to see that the smoothing spline method is not capable of simultaneously suppressing noise and preserving sharp edges. as shown in Fig. 2(c). And it cannot be remedied by adjusting the corresponding smoothing parameter as using large values of smoothing parameter will over-smooth edges and using small values of smoothing parameter can not remove noise. In contrast, all three other methods: Huber-TV method, TV method and our wavelet frame based method can preserve sharp edges while removing most noises, as shown in Fig. 2(d)–(f), respectively. However, a close-up examination (Fig. 2(g)–(i)) shows that the results from these three methods differs quite noticeably in terms of visual quality. In the result from Huber-TV method shown in Fig. 2(g), the supposedly straight planes are distorted to arc surfaces, due to the introduction of the parameter β used for smoothing ℓ_1 norm. It is noted that such artifacts can be alleviated by using smaller β. However, the convergence of the corresponding solver, gradient descent algorithm, will be extremely slow if the value of β is small. The result from TV method also suffers from noticeable artifacts. One is the well-known "staircase" type of artifacts; the other is the rounded corners as shown in Fig. 2(h). It is easy to see that the result from our frame based algorithm (Fig. 2(i)) has the least noticeable artifacts.

3.3. Experiments on range data sets

In this section, we conduct experiments on both synthesized and real range data sets to evaluate the performance of our proposed wavelet frame based method in the presence of noise. As the tested range data sets have resolution $2^J\times 2^J$ where $J=7$ or 8, the scaling parameter h is set to $1/2^J$.

The first experimental range data set is synthesized for a simple indoor scene with objects of typical shapes. The photometric image is shown in Fig. 3(a) and the corresponding range image is shown in Fig. 3(b), where the darker intensity denotes the less distance away from range camera. The surface from the full range data set with size 256×256 is shown in Fig. 4(a). The range date set used for the input of the reconstruction is a 5% randomly selected subset of the range data set followed by the corruption of Gaussian noise, as shown in (4)(b) using nearest neighbor interpolation. The reconstructed results from three previous methods and our proposed method are shown in Fig. 4(c)–(f), respectively.

The second experimental range data set is a real data set from the online USF range image database [43], which is originally attributed to the CESAR lab of Oak Ridge national laboratory at Tennessee. The range image is of size 128×128. The input used in our experiments is similar to the ones considered in [44]: only a number of horizontal scan lines (one of each seven horizontal scan lines) available and corrupted with Gaussian noise ($\sigma=1$). Fig. 5 shows the surface from the latent full data set, the result from partial noisy data set using nearest neighbor interpolation, and the results from the same partial noisy data set using three previous algorithms and our proposed algorithm.

The experimental results on the above two sparse noisy range data sets clearly indicate the better performance of our proposed algorithm over three previously developed algorithms for sparse and noisy range data sets. Similar to previous

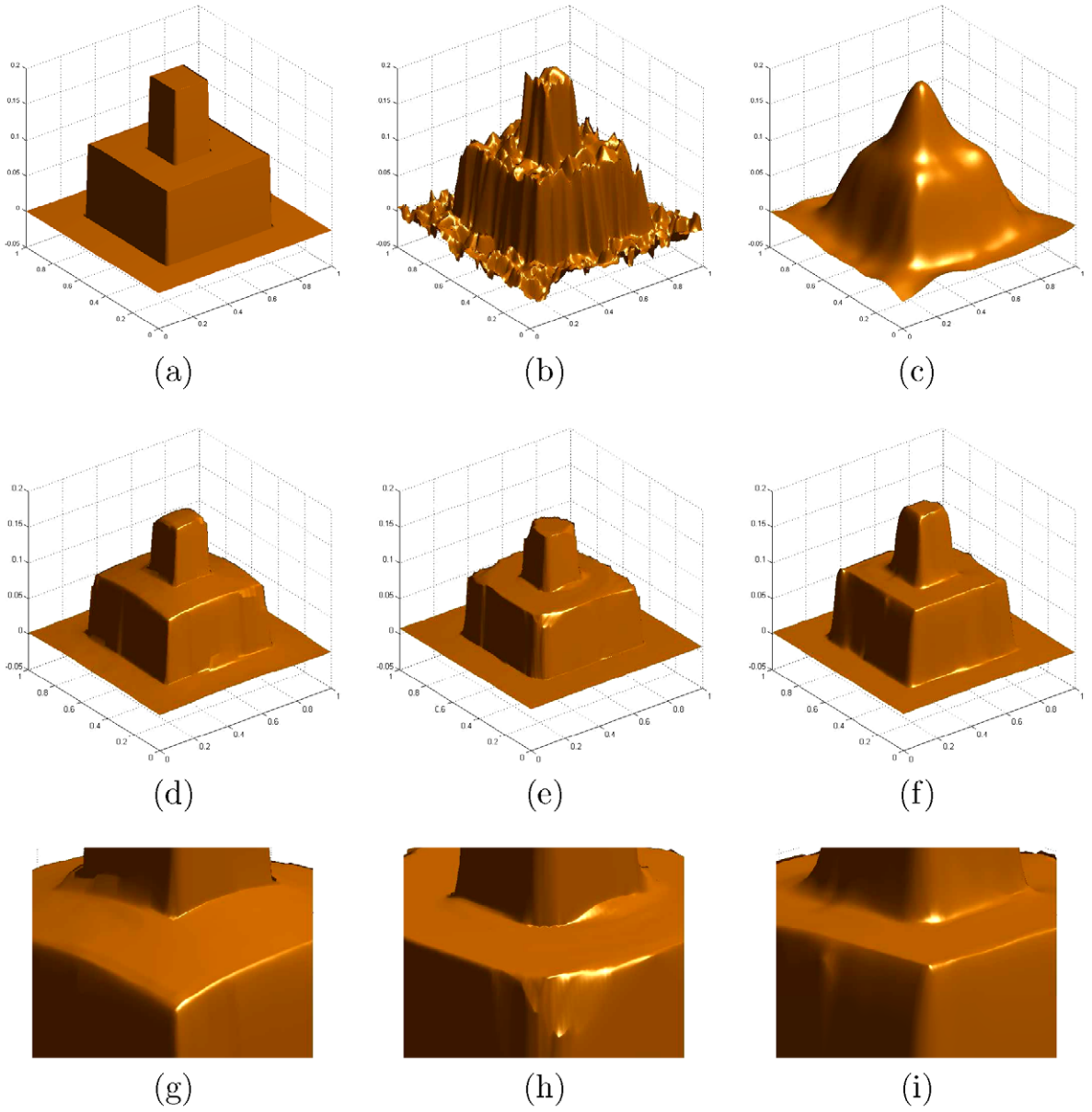

Fig. 2. Reconstruction of a noisy "wedding cake" shape. (a) Original latent surface. (b) The surface reconstructed from a noisy sample set of the original surface using nearest neighbor interpolation. (c) The reconstructed surface by the smoothing spline method (3) with $\lambda = 196$ using the same sample set. (d), (e) and (f) are the results obtained from Huber-TV method (19), TV-based method (18) and our wavelet frame based method (8) with the ℓ_2 fitting term, respectively; the employed regularization parameters are $\lambda = 20,\ 0.02,\ 0.005$, respectively. (g)–(i) show one portion of surfaces in (d)–(f), respectively.

Fig. 3. The photometric image and range image of a simple indoor scene.

Fig. 4. Reconstruction of a noisy range map. (a) Original range map surface. (b) The surface from a sparse noisy sample set using nearest neighbor interpolation. (c)–(f) are, respectively, the reconstructions obtained by the smoothing spline (3), the Huber-TV method (19), the TV-based method (18) and the wavelet frame based method (8) with the ℓ_2 fitting term; the employed regularization parameters are $\lambda = 132,\ 98,\ 2,\ 1$, respectively.

experimental results, the smoothing spline method clearly is not suitable for solving general piecewise surface fitting problems as it does not preserve shape edges. Both Huber-TV method and TV method preserve sharp edges much better than smoothing spline method does. However, there are noticeable artifacts in the surfaces reconstructed by these two methods, specially those "staircase" artifacts. Although the usage of large values of β in Huber-TV method may alleviate the staircase artifacts, but the sharp discontinuities of the surface will be smoothed out at the same time. Overall, our wavelet frame based method yields the result with sharp edges and with less visible artifacts than that of other methods.

One main argument why wavelet frame based method performs better than TV (and Huber-TV) method is that TV regularization used in these two methods only utilizes the gradients of the underlying function while frame based regularization (the ℓ_1-norm of canonical frame coefficients) used in our method encodes additional information regarding higher-order derivatives. It is noted that the two filters $\boldsymbol{h}_1,\ \boldsymbol{h}_2$ in (7) are indeed the first and second order difference operators, respectively. The advantages of incorporating higher-order derivative information in the regularization term to suppress the staircase artifacts in the result are also observed in some recent research works (*e.g.* [45,46]). In our frame based approach, the regularization on both lower-order and higher-order derivative information are elegantly fused together in one tight frame system, and the resulting surface does not suffer from staircase artifacts.

In the applications with data points only available at very sparse locations or only scanned in a very low-resolution, *e.g.* the 3D points from photometric images via computer vision techniques or range image captured by cheap time-of-flight rangefinders, a straightforward application of our frame-based algorithm on such data sets may not always lead to a satisfactory result. Because the regularization term is not strong enough to stitch all data together to produce a valid surface due to the fact that too few data constraints are available. In such a case, a preprocessing process on the inputed data is proposed to increase the data size before the actual frame-based algorithm is applied. The preprocessing procedure is as follows. First, we use cubic interpolation to approximate the given data on a finer grid. Considering that the reliable data points on the grid are those close enough to the inputed data, we then only add those reliable data points to the inputed data set to form a new data set. Then this new data set is used as the input of our wavelet frame based method. To illustrate the very low requirement of our proposed method on the sample size of needed range data set, we consider the case of only a very small number

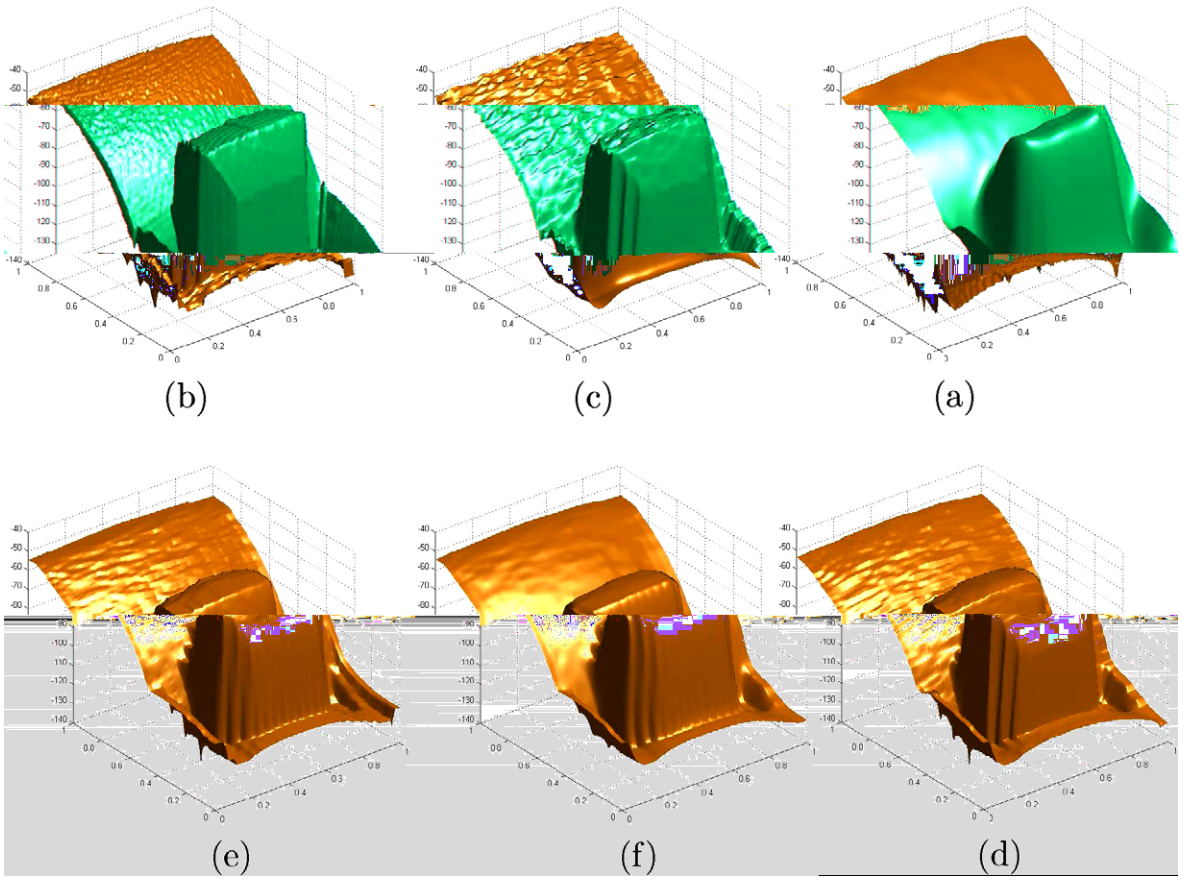

Fig. 5. Reconstruction on a USF data set. (a) The surface from the original data set; (b) the surface from partially scanned noisy data using nearest neighbor interpolation. (c)–(f) are the results from the partially scanned noisy data set using smoothing spline (3), Huber-TV method (19), the TV-based method (18) and wavelet frame based method (8), respectively; the employed regularization parameters are $\lambda = 98,\ 1.5,\ 2,\ 1.5$, respectively.

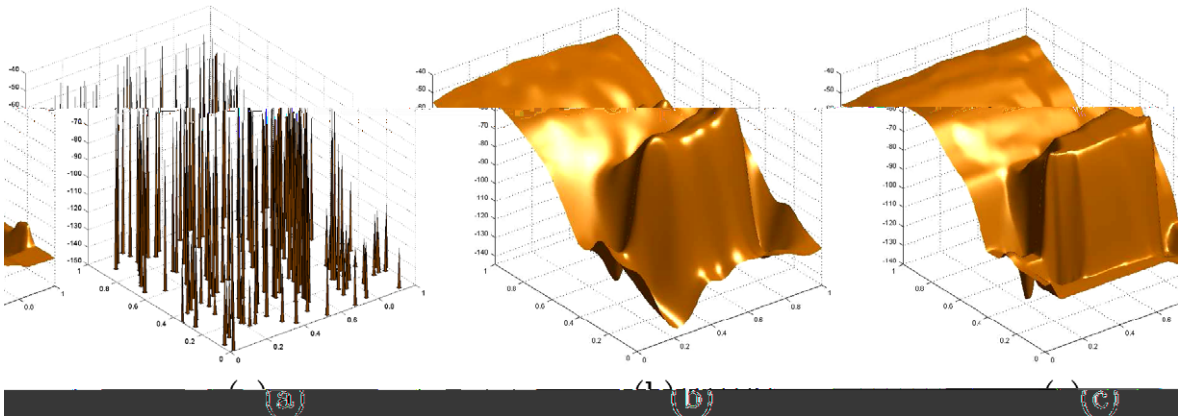

Fig. 6. Reconstruction on a very sparse data set. (a) Sparse data sites and the corresponding noisy functional values; (b) the result from smoothing spline method (3) without preprocessing ($\lambda = 66$). (c) The result from wavelet frame based method (8) with the preprocessing step ($\lambda = 2$).

of data points available from the data set shown in Fig. 5 (163 points out of the full set with 16,384 points). Fig. 6 shows the noisy functional values, and the surfaces reconstructed from this sparse data set by the smoothing spline method and our wavelet frame based method with the proposed preprocessing step.

Finally, one experiment is done on the surface with much more complicate geometrical structures. This data set, taken from the online OSU range image database [47], is shown in of Fig. 7(a), which gives the depth map of a Buddha statue. Only

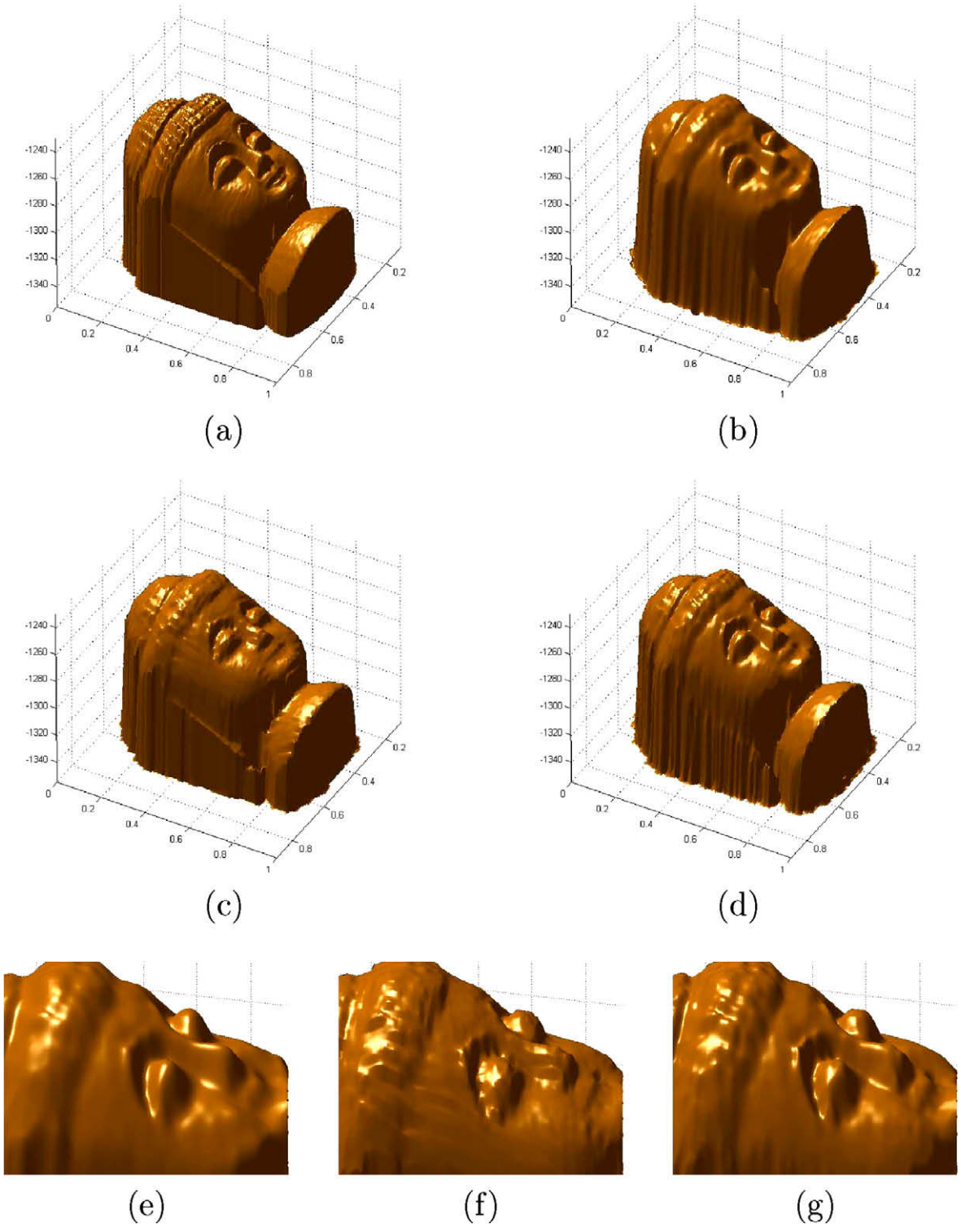

Fig. 7. Reconstruction on a Buddha statue. (a) The surface from the original data set; (b)–(d) are the results from a sparse noisy data set using smoothing spline (3), Huber-TV method (19) and wavelet frame based method (8), respectively; the employed regularization parameters are $\lambda = 1.3,\ 0.3,\ 0.06$, respectively. (e)–(g) are one portion of (b)–(d), respectively.

a noisy subset of the original data set (20%) is used as the input. The results from smoothing spline method, Huber-TV method and our method are shown in Fig. 7. The reconstruction by TV method is not shown as it appears nearly the same as that by Huber-TV method. Similarly, the result from our method is the one with least noticeable artifacts.

3.4. Reconstruction for data with outliers

In addition to additive noise, there could be also a lot of outliers in the range data. Dynamic environment changes and the physical limitations of range camera could introduce a lot of outliers in the captured range image (see *e.g.* [29]), and even state-of-art vision techniques will also unavoidably give a lot of false 3D points when inferring 3D depth of feature points from photometric images.

In this section, numerical experiments are conducted on two range data sets corrupted with both Gaussian noise and outliers. The results from wavelet frame based method (8) with ℓ_2 fitting term are compared against that with ℓ_1 fitting term. To better evaluate the performance of ℓ_2 fitting term and ℓ_1 fitting term on suppressing outliers, we use different regularization

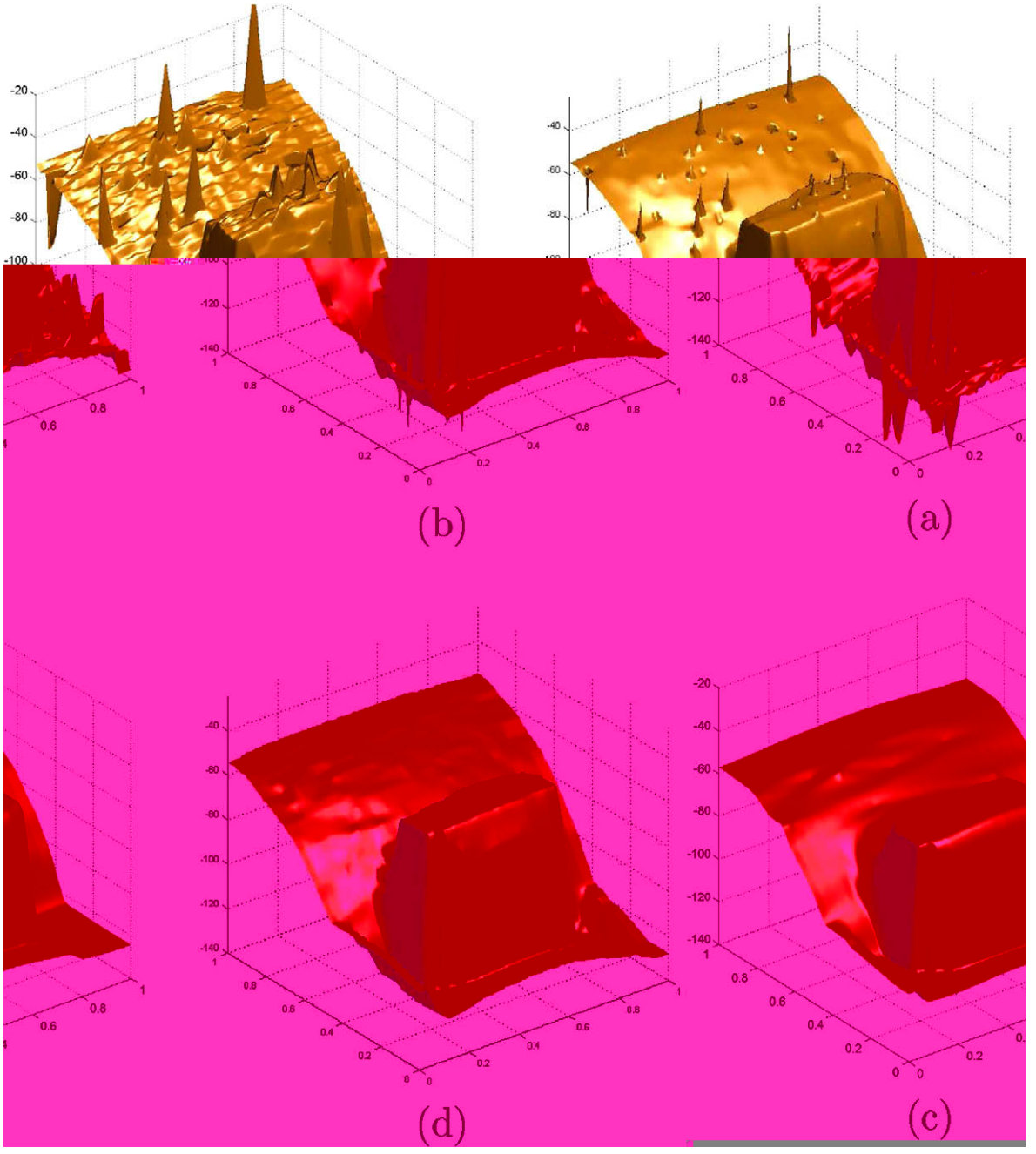

Fig. 8. Reconstruction on data corrupted with both Gaussian noise and outliers. (a) The noisy data with outliers; (b), (c) the results from wavelet frame based method (8) with ℓ_2 fitting term ($\lambda = 1,\ 10$, respectively); (c) the result from wavelet frame based method (8) with ℓ_1 fitting term ($\lambda = 0.5$).

parameters for two regularization terms such that both corresponding methods give the same ℓ_2 value of residual error. The inputed data with outliers and the reconstructed surfaces from these two methods are shown in Figs. 8 and 9. It is seen that the method with ℓ_2 fitting term either does not suppress outliers when using a small regularization parameter as the resulting surface tends to interpolate the outliers; or produces a over-smoothed surface when using a large regularization parameter. See Figs. 8(b), (c) and 9(b), (c) for the visual comparison.

3.5. Discussions

In this paper, a new method for reconstructing piecewise smooth surfaces from sparse range data is proposed by exploiting the sparsity of piecewise functions in wavelet tight frame domain. And the resulting minimization can be efficiently

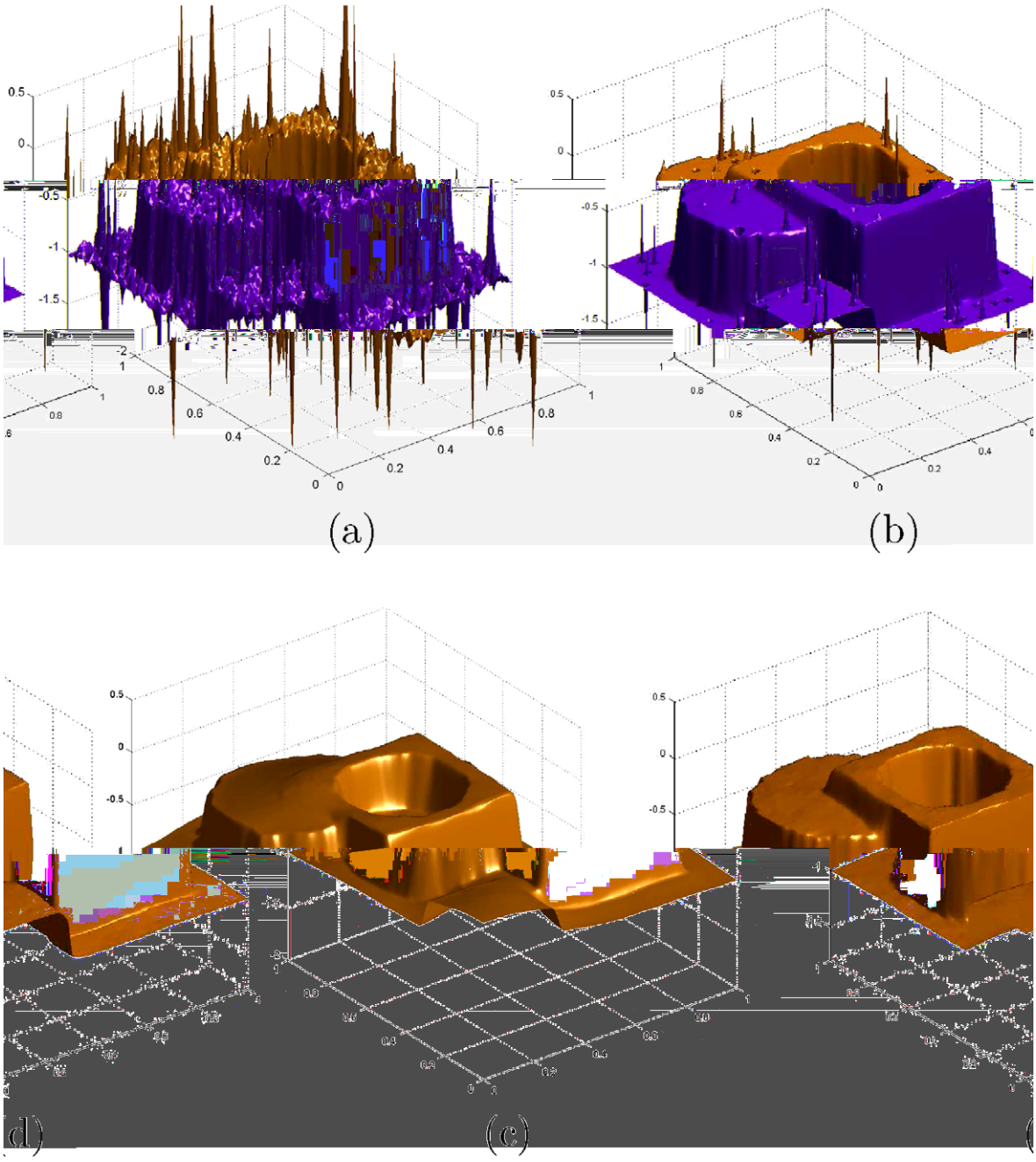

Fig. 9. Reconstruction on data corrupted with both Gaussian noise and outliers. (a) The noisy data with outliers; (b), (c) the results from wavelet frame based method (8) with ℓ_2 fitting term ($\lambda = 0.1, 0.5$, respectively); (d) the result from wavelet frame based method (8) with ℓ_1 fitting term ($\lambda = 1.2$).

solved by the split Bregman method. Through various experiments, the proposed method demonstrates its strong robustness to both additive noise and outliers and outperforms many previous developed methods in terms of the visual quality of results. The robustness to noise and outliers are particularly important for solving the problem of surface fitting using range data from vision techniques as there usually exist a lot of falsely detected 3D points in these range data sets. Furthermore, it is shown that the proposed method is even applicable for very sparse range data sets, which makes it a very attractive post-process to improve the quality (*e.g.* signal-to-noise ratio, resolution) of data sets from low-cost time-of-flight rangefinders. In future, we are interested in investigating the possibility of incorporating our surface fitting algorithm into the depth computation of image feature points by vision techniques for further performance improvements. Also, the extension of our current approach to address more general surface fitting problems will be considered in the near future.

Acknowledgments

We would like to thank two anonymous reviewers for their comments which greatly improve the presentation of this paper. This work is partially supported by the NUS ARF Grant R-146-000-126-112. The third author also would like to thank the support by the Wavelets and Information Processing Programme of the Centre for Wavelets, Approximation and Information Processing and Temasek Laboratories, National University of Singapore.

References

[1] J.-F. Cai, S. Osher, Z. Shen, Split Bregman methods and frame based image restoration, Multiscale Model. Simul., in press.
[2] T. Goldstein, S. Osher, The split Bregman method for $L1$-regularized problems, SIAM J. Imaging Sci. 2 (2) (2009) 323–343.
[3] M. Gross, F. Pfister, Point-Based Graphics, Morgan kaufmann, 2007.
[4] M. Johnson, Z. Shen, Y. Xu, Scattered data reconstruction by regularization in B-spline and associated wavelet spaces, J. Approx. Theor. 159 (2) (2009) 197–223.
[5] J. Carr, R. Beatson, J. Cherrie, T. Mitchell, W. Fright, B. McCallum, T. Evans, Reconstruction and representation of 3D objects with radial basis functions, in: Computer Graphics (SIGGRAPH 2001 Proceedings), 2001, pp. 67–76.
[6] D. Terzopoulos, Regularization of inverse visual problems involving discontinuities, IEEE Trans. Pattern Anal. Mach. Intell. 8 (4) (1986) 413–424.
[7] X. He, L. Shen, Z. Shen, A data-adaptive knot selection scheme for fitting splines, IEEE Signal Proc. Lett. 8 (5) (2001) 137–139.
[8] M. Johnson, Scattered data interpolation from principal shift-invariant spaces, J. Approx. Theor. 113 (2) (2001) 172–188.
[9] Z. Shen, S. Waldron, Scattered data interpolation by box splines, in: Third International Congress of Chinese Mathematicians, Part 1, 2, Vol. 2, AMS/IP Stud. Adv. Math., 42, Part. 1, Amer. Math. Soc., Providence, RI, 2008, pp. 749–767.
[10] H. Dinh, G. Turk, G. Slabaugh, Reconstructing surfaces using anisotropic basis functions, in: International Conference on Computer Vision (ICCV), 2001, pp. 606–613.
[11] R. Stevenson, B. Schmitz, E. Delp, Discontinuity preserving regularization of inverse visual problems, IEEE Trans. Syst. Man Cyb. 3 (1994) 455–469.
[12] I. Gijbels, A. Lambert, P. Qiu, Edge-preserving image denoising and estimation of discontinuous surfaces, IEEE Trans. Pattern Anal. Mach. Intell. 28 (7) (2006) 1075–1087.
[13] B. Dong, J. Ye, S. Osher, I. Dinov, Level set based nonlocal surface restoration, Multiscale Model. Simul. 7 (2) (2008) 589–598.
[14] E. Candes, J. Romberg, T. Tao, Robust uncertainty principles: exact signal reconstruction from highly incomplete frequency information, IEEE Trans. Inform. Theor. 52 (2) (2006) 489–509.
[15] M. Elad, P. Milanfar, R. Rubinstein, Analysis versus synthesis in signal priors, Inverse Probl. 23 (3) (2007) 947–968.
[16] L. Rudin, S. Osher, C. Fatemi, Nonlinear total variation based noise removal algorithms, Physica D 60 (1992) 259–268.
[17] T. Goldstein, X. Bresson, S. Osher, Geometric applications of the split Bregman method: segmentation and surface reconstruction, Tech. Rep., CAM Report, UCLA, 2009.
[18] L. Borup, R. Gribonval, M. Nielsen, Bi-framelet systems with few vanishing moments characterize Besov spaces, Appl. Comput. Harmon. Anal. 17 (1) (2004) 3–28.
[19] I. Daubechies, B. Han, A. Ron, Z. Shen, Framelets: MRA-based constructions of wavelet frames, Appl. Comput. Harmon. Anal. 14 (1) (2003) 1–46.
[20] B. Han, Z. Shen, Dual wavelet frames and Riesz bases in Sobolev spaces, Constr. Approx. 29 (3) (2009) 369–406.
[21] A. Ron, Z. Shen, Affine systems in $L2(\mathbb{R}^d)$: the analysis of the analysis operator, J. Funct. Anal. 148 (2) (1997) 408–447.
[22] I. Daubechies, Ten lectures on wavelets, Society for Industrial and Applied Mathematics (SIAM), Philadelphia, PA, 1992.
[23] S. Mallat, A Wavelet Tour of Signal Processing, Academic Press, Inc., San Diego, CA, 1998.
[24] J.-F. Cai, R. Chan, L. Shen, Z. Shen, Restoration of chopped and nodded images by framelets, SIAM J. Sci. Comput. 30 (3) (2008) 1205–1227.
[25] J.-F. Cai, R.H. Chan, Z. Shen, A framelet-based image inpainting algorithm, Appl. Comput. Harmon. Anal. 24 (2) (2008) 131–149.
[26] J.-F. Cai, H. Ji, C. Liu, Z. Shen, Blind motion deblurring using multiple images, J. Comput. Phys. 228 (14) (2009) 5057–5071.
[27] J.-F. Cai, H. Ji, C. Liu, Z. Shen, Blind motion deblurring from a single image using sparse approximation, in: IEEE Conference on Computer Vision and Pattern Recognition (CVPR), 2009.
[28] A. Chai, Z. Shen, Deconvolution: a wavelet frame approach, Numer. Math. 106 (4) (2007) 529–587.
[29] M. Umasuthan, A. Wallace, Outlier removal and discontinuity preserving smoothing of range data, in: IEE Proceedings of the Vision Image Signal Process, No. 3, 1996, pp. 191–200.
[30] T.F. Chan, S. Esedoglu, Aspects of total variation regularized $L1$ function approximation, SIAM J. Appl. Math. 65 (5) (2005) 1817–1837 (electronic).
[31] M. Nikolova, A variational approach to remove outliers and impulse noise, J. Math. Imaging Vis. 20 (2004) 99–120.
[32] S. Osher, M. Burger, D. Goldfarb, J. Xu, W. Yin, An iterative regularization method for total variation-based image restoration, Multiscale Model. Simul. 4 (2) (2005) 460–489 (electronic).
[33] W. Yin, S. Osher, D. Goldfarb, J. Darbon, Bregman iterative algorithms for ℓ_1-minimization with applications to compressed sensing, SIAM J. Imaging Sci. 1 (1) (2008) 143–168.
[34] J.-F. Cai, S. Osher, Z. Shen, Linearized Bregman iterations for frame-based image deblurring, SIAM J. Imaging Sci. 2 (1) (2009) 226–252.
[35] E. Esser, Applications of lagrangian-based alternating direction methods and connections to split Bregman, Tech. Rep., CAM Report, UCLA, 2009.
[36] S. Setzer, Split Bregman algorithm, Douglas–Rachford splitting and frame shrinkage, in: Proceedings of the Second International Conference on Scale Space Methods and Variational Methods in Computer Vision 2009, 2009.
[37] D. Gabay, B. Mercier, A dual algorithm for the solution of nonlinear variational problems via finite-element approximations, Comput. Math. Appl. 2 (1976) 17–40.
[38] R. Glowinski, A. Marroco, Sur lapproximation par elements finis dordre un, et la resolution par penalisation-dualite dune classe de problemes de Dirichlet nonlineaires, Rev, Francaise dAut., Inf. Rech. Oper R-2 (1975) 41–76.
[39] J. Douglas, H.H. Rachford, On the numerical solution of heat conduction problems in two and three space variables, Trans. Am. Math. Soc. 82 (1956) 421–439.

[40] J. Eckstein, Splitting methods for monotone operators with applications to parallel optimization, Ph.D. thesis, Massachusetts Institute of Technology, 1989.
[41] P.-L. Lions, B. Mercier, Splitting algorithms for the sum of two nonlinear operators, SIAM J. Numer. Anal. 16 (6) (1979) 964–979.
[42] T.F. Chan, J. Shen, Image processing and analysis: variational, PDE, wavelet, and stochastic methods, Society for Industrial and Applied Mathematics (SIAM), Philadelphia, PA, 2005.
[43] <http://marathon.csee.usf.edu/range/DataBase.html>.
[44] G. Chen, G. Dudek, L. Torres-Mendez, Scene reconstruction with sparse range information, in: The Second Canadian Conference on Computer and Robot Vision, 2005, Proceedings, 2005, pp. 444–451.
[45] T. Chan, A. Marquina, P. Mulet, High-order total variation-based image restoration, SIAM J. Sci. Comput. 22 (2000) 503–516.
[46] S. Setzer, G. Steidl, Variational methods with higher order derivatives in image processing, Approximation, vol. XII, Nashboro Press, Brentwood, 2008, pp. 360–386.
[47] <http://sampl.ece.ohio-state.edu/data/3DDB/RID/index.htm>.